Solar Physics (2005) 226: 337–357
DOI: 10.1007/s11207-005-6877-2

THE INTERPLANETARY RESPONSES TO THE GREAT SOLAR ACTIVITIES IN LATE OCTOBER 2003

YUMING WANG[1], PINZHONG YE[1], GUIPING ZHOU[2], SHUJUAN WANG[2], S. WANG[1], YIHUA YAN[2] and JINGXIU WANG[2]
[1]*School of Earth & Space Science, University of Science & Technology of China, Hefei, Anhui 230026, China*
(e-mail: ymwang@ustc.edu.cn)
[2]*National Astronomical Observatories of China, Beijing 100012, China*

(Received 13 July 2004; accepted 15 November 2004)

Abstract. Based on the observations of the Sun and the interplanetary medium, a series of solar activities in late October 2003 and their consequences are studied comprehensively. Thirteen X-ray flares with importance greater than M-class, six frontside halo coronal mass ejections (CMEs) with span angle larger than 100° and three associated eruptions of filament materials are identified by examining lots of solar observations from October 26 to 29. All these flares were associated with type III radio bursts, all the frontside halo CMEs were accompanied by type II or type II-like radio bursts. Particularly, among these activities, two major solar events caused two extraordinary enhancements (exceeding 1000 particles/(cm^2 s^{-1} ster^{-1} Mev^{-1}) of solar energetic particle (SEP) flux intensity near the Earth, two large ejecta with fast shocks preceding, and two great geomagnetic storms with *Dst* peak value of −363 and −401 nT, respectively. By using a cross correlation technique and a force-free cylindrical flux rope model, the October 29 magnetic cloud associated with the largest CME are analyzed, including its orientation and the sign of its helicity. It is found that the helicity of the cloud is negative, contrary to the regular statistical pattern that negative- and positive-helical interplanetary magnetic clouds would be expected to come from northern and southern solar hemisphere. Moreover, the relationship between the orientation of magnetic cloud and associated filament is discussed. In addition, some discussion concerning multiple-magnetic-cloud structures and SEP events is also given.

1. Introduction

In the current solar cycle, the recent solar maximum appeared in 2000–2002 approximately, and it entered the descending phase around 2003. The interplanetary transient structures and geomagnetic disturbances became fewer and weaker obviously in 2003 according to observations of solar wind and interplanetary magnetic field from the ACE spacecraft and the geomagnetic indices. However, a series of surprising events occurred in late 2003. Many consequences, such as solar energetic particles (SEPs), radio bursts, shocks, interplanetary ejecta, magnetic clouds (MCs), geomagnetic storms, and so on, were produced by these violent solar activities, and therefore greatly changed the space weather near the Earth.

There were about 110 X-ray flares, including 35 M-class and 7 X-class flares (two of them were more intense than X10), 45 coronal mass ejections (CMEs) from 19 to 31 October 2003, which producing ∼3 SEP events, a series of interplanetary

ejecta near the Earth, and three large geomagnetic storms. The case that several solar activities occurred within a short interval is often observed (Webb *et al.*, 2000; Nitta and Hudson, 2001; Burlaga *et al.*, 2001; Burlaga, Plunkett, and St. Cyr, 2002; Wang, Wang, and Ye, 2002), especially near solar maximum. Nevertheless, the large activities occurring with such a high frequency as the 2003 October events and causing such violent geoeffectiveness are rare. So frequent occurrence of large solar activities make the relation between solar activities and interplanetary disturbances more intricate.

The "Bastille" event on July 14, 2000 received attention due to its violent energy released from the Sun and the notable effect on the Earth (Lepping *et al.*, 2001; Smith *et al.*, 2001). That CME associated with a X5.7 X-ray flare produced a magnetic cloud with speed of $\geq$1100 km s^{-1} at 1 AU, and caused a double-peak structure super-storm (*Dst* peak less than -300 nT) two days later. However, since there was no other great solar activity during that period, it is easy to identify the interplanetary response to the "Bastille" event. Some events studied by Gonzalez and Tsurutani (1987) and Tsurutani *et al.* (1988) are similar relatively isolated major events. The cause–effect chains in these events are clear and definite. How about the October 2003 multiple events? This is the main aim of this paper.

Although there were many activities from 19 to the end of October 2003, the major events, including the only two super X-ray flares ($\geq$X10) and three SEPs events, occurred during October 26–29, 2003, and produced two great geomagnetic storms ($Dst \leq -300$ nT) 1–2 days later. Thus, we only investigate the observations from 26 to 29 October (for interplanetary data, it is extended to 1 November) to try to identify the major solar activities and their interplanetary responses and geoeffectiveness. The following two sections are devoted to presenting the solar activities, interplanetary phenomena and geomagnetic storms. In Section 4, we summarize the paper and give some discussion.

2. Solar Activities

From 26 to 29 October, there were 13 X-ray flares with class above M-class and 7 CMEs with span angle larger than 100° (thereafter treated as halo CMEs). Table I gives an overview of these solar activities and the relations between them.

All of the X-class flares were associated with halo CMEs, and half of all frontside halo CMEs were companied by giant filament disappearances. The first X1.2 flare beginning at 05:57 UT on 26 October occurred at S15 E44 in active region (AR) 10486. A halo CME first appeared on the east-southern in the field of view (FOV) of the LASCO/C2 at 06:54 UT. The direction and the time of this CME suggest that the CME is related to the flare. The projected speed of it is estimated as 1370 km s^{-1}. On the same day, another X-class flare also associated with a halo CME burst at N02W38 from 17:21 UT in AR 10484. The related CME was preceded by a wide bright loop front with speed of $\sim$1537 km s^{-1} extended over the west rapidly in

TABLE I

List of the solar activities during 26–29 October 2003.

		X-ray flares					Halo CMEs				Filament eruptions	
No.	Date	Begin	Maximum	End	Class	Location/AR	Time	Width	Speed	F[a]	Onset	Location
1	October 26	0557	0654	0733	X1.2	S15E44/486	0654	>200	1370	Y	–	–
2	October 26	1415	1420	1424	M1.0	N05W33/484	–	–	–	–	–	–
3	October 26	1721	1819	1921	X1.2	N02W38/484	1754	>171	1537	Y	1700	AR10484-486
4	October 26	2134	2140	2148	M7.6	N01W38/484	–	–	–	–	–	–
5	October 27	0412	0439	0508	M1.2	N00W44/484	–	–	–	–	–	–
6	October 27	0751	0833	0924	M2.7	N00W45/484	0830	144	1322	Y	–	–
7	October 27	0921	0927	0932	M5.0	S16E26/486	–	–	–	–	–	–
8	October 27	1227	1243	1252	M6.7	S17E25/486	–	–	–	–	–	–
9	October 27	2146	2151	2205	M1.9	N08E09/488	–	–	–	–	–	–
10	October 28						1054	147	1054	Y	–	–
11	October 28	0951	1110	1124	X17.2	S16E08/486	1130	360	2459	Y	1123	AR10484-486
12	October 29	0026	0151	0208	M1.1	S18E08/486	–	–	–	–	–	–
13	October 29	0408	0511	0554	M3.5	S17E06/486	–	–	–	–	–	–
14	October 29	–	–	–	–	–	1017	114	922	N	–	–
15	October 29	2037	2049	2101	X10.0	S15W02/486	2054	360	2029	Y	2048	AR10486-488

[a]Frontside (Y) or not (N).

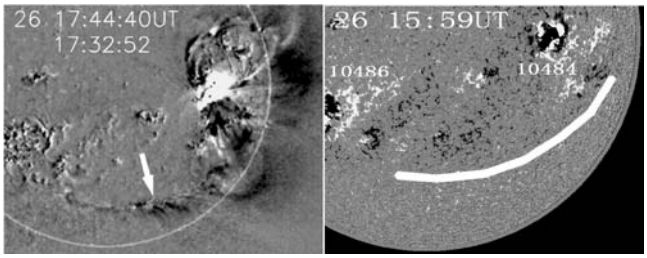

Figure 1. Running difference image of EIT 195Å (*left*) on October 26 and the corresponding photospheric magnetic field observations of MDI (*right*). *White arrow* marks the polar crown filament, which is denoted by the *white line* in the MDI image.

LASCO observations. The EIT movie shows that the companied solar activities included the material ejections of a long polar crown filament, which connected with AR 10484 and 10486 (as marked by the white arrow in Figure 1). The filament was in the east-west direction, and the observed line of sight magnetic field was positive at the south side of filament channel and negative on the other side according to the MDI observations (Figure 1, right panel).

The flares occurring on 27 October were all smaller than X-class. Only a M2.7 flare appearing at N00 W45 in AR 10484 during 07:51 to 09:24 UT was companied by a halo CME. There was no obvious associated filament eruption. The front of this CME arrived at $\sim$1.5 R_s at 08:20 UT according to the EIT movie, and entered the FOV of LASCO at 08:30 UT. The projected speed was about 1322 km s^{-1}.

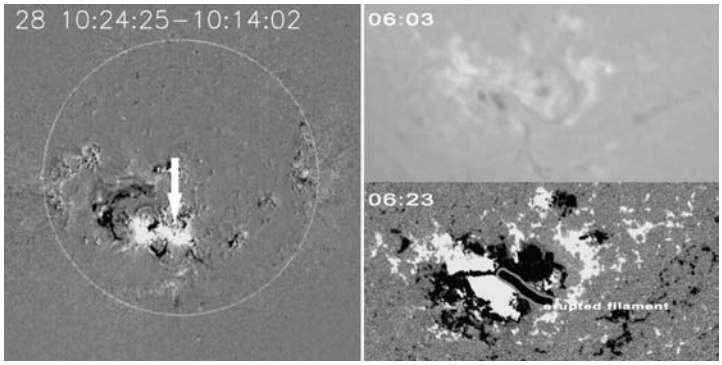

Figure 2. Running difference image of EIT 195Å (*left panel*) and the corresponding H_α image from Yunnan Astronomical Observatory (*right upper panel*) and the photospheric magnetic field observations of MDI (*right lower panel*). *White arrow* marks the giant filament, which is denoted by the thick *black line* in the MDI image.

On 28 October, there was only one large X-ray flare, which was extremely violent with class of X17.2. This super flare began at 09:51 UT and ended at 11:24 UT in AR 10486. Simultaneously, a giant filament connecting with AR 10484 and 10486 erupted. The main erupted part was in AR 10486 as marked by the white arrow in the left column of Figure 2. This erupted filament was approximately in northeast-southwest orientation as shown clearly in the H_α image in Figure 2. Based on the MDI observations, the magnetic field arcades over the filament directed from south-east to north-west roughly. Following it, at 11:30 UT, a bright full halo CME with a very fast outward speed of >2000 km s^{-1} appeared in the FOV of LASCO/C2. In addition to this violent event, there was another small halo CME appearing in the south-east in the FOV of LASCO at 10:54 UT. Compared to the 11:30 UT CME, this preceding CME was narrow (span angle was about 124°) and faint though its speed was larger than 1000 km s^{-1}. This CME seemed to also be related to the X17.2 flare.

The last super X-ray flare (X10.0) in October occurred on the 29th. This flare burst at S15 W02 in AR 10486 from 20:37 to 21:01 UT. As the 28 October super flare, it was also associated with a violent halo CME (Figure 3), which also involves

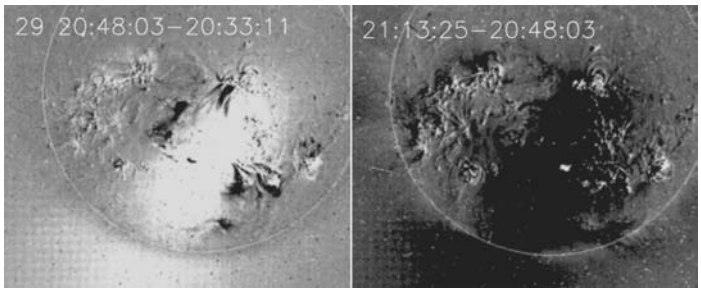

Figure 3. Running difference images of EIT 195Å.

a giant filament disappearance. From the EIT movie, the filament spanned two active regions 10486 and 10488, which was not very clear in H_α images. Its eruption seemed to begin at 20:48 prior to the CME's first appearance (20:54 UT) in LASCO/C2. This is consistent with the estimated CME speed that was larger than 2000 km s^{-1}. As for another halo CME at 10:17 UT, there was no obvious signature to prove it originated on the frontside. Therefore, it is considered backside and has no geoeffectiveness.

Events 1, 3, 6, 10, 11 and 15 involved both flares and CMEs, and they contained all X-class flares and all frontside halo CMEs. Thus, these major solar events were studied to find their interplanetary responses.

3. Interplanetary Responses

An overview of the interplanetary responses from 26 October to 1 November is shown in Figure 4. Around October 28–30, the observations of solar wind plasma are not very reliable. The data plotted in Figure 4 during that interval is directly obtained from Dr. R. Skoug (ACE/SWEPAM), Dr. T. Zurbuchen (ACE/SWICS), and Dr. T. Terasawa (Geotail/PWI). The first seven panels are plotted based on the ACE observations and the last two panels of the radio spectrum are from the Wind spacecraft. The time (at the maximum of flares) of the solar activities listed in Table I are denoted by the vertical lines. The solid lines mean that the event involved both flare and halo CME, and the thick solid lines indicate that flare was greater than X1-class. The dashed lines mean there was no associated halo CME.

The interplanetary responses roughly have two categories. One is the immediate response, and another is the delayed response. Solar radio bursts and SEPs belong to immediate responses because they propagate rapidly in the interplanetary medium and can arrive at 1 AU quickly. Interplanetary ejecta, CME-driven shocks and their associated geomagnetic storms will arrive at 1 AU after several days, usually within 3–5 days (Webb *et al.*, 2000), sometimes within 2 days (Wang *et al.*, 2002). Thus, they can be treated as delayed responses.

3.1. Solar radio bursts

From Figure 4, some immediate responses are obvious as well as their corresponding solar activities. Almost all the flares were associated with type III radio bursts, and all of the frontside halo CMEs were accompanied by type II or type II-like radio bursts. In several events, drifting pulsation structures (DPSs) and type IV radio bursts also appeared. To identify these solar radio bursts and their sources, we studied on them in a multi-wavelength range over a large coronal region across the microwave, the decimetric wavelength, the metric wavelength and even to much longer wavelength. The data of the solar radio fast dynamic spectrometer (1–7.6 GHz) was recorded by Huairou Station of NAOC in Beijing. Also on the

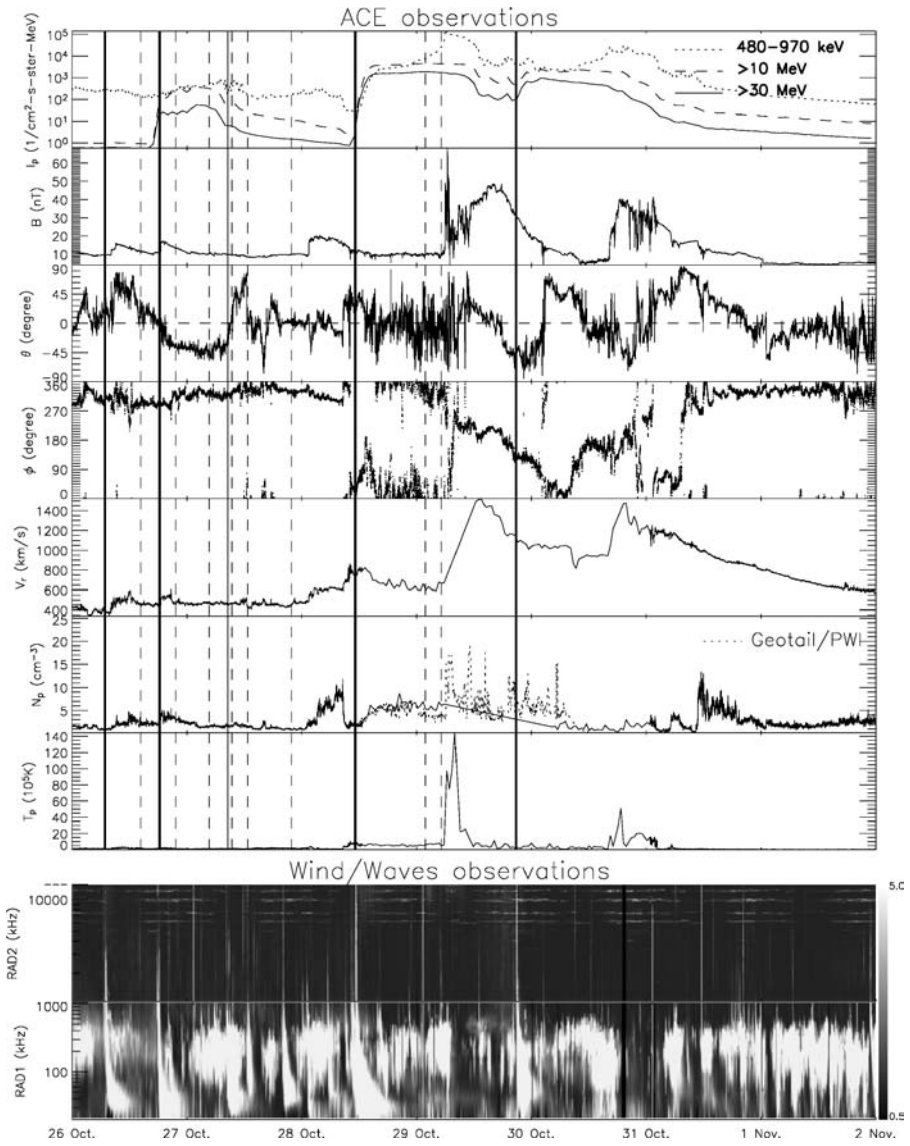

Figure 4. An overview of the interplanetary observations from October 26 to November 1, 2003. The first seven panels are plotted for energetic proton intensities I_p, magnetic field strength B, the elevation θ and azimuthal ϕ of field direction, solar wind speed along the Sun–Earth line V_r, proton density N_p and proton temperature T_p, based on the ACE observations. The last two panels present the interplanetary radio bursts based on the *Wind/Waves* observations. The time (the maximum of flares are used) of the solar activities listed in Table I are denoted by the *vertical lines*. The *solid lines* mean that the activity contained flare and halo CME and the thicker ones indicate the flare was greater than X1-class. The *dashed lines* mean the flare without associated halo CME.

Internet the other dynamic spectra from a few GHz to a few kHz were prepared by several radio instruments including RAD2 data of *Wind/Waves* (1.075 kHz–13.825 MHz), DAM/Nancay of France (20–70 MHz), Learmonth Spectrograph of Australia (25–180 MHz), Hiraiso of Japan (25–2500 MHz) and PHOENIX-2 of Switzerland (0.1–4.0 GHz). Based on time associations and phenomenological arguments shown from the broad radio spectra (Figures 5–7) later, we believe that the type III bursts in the band RAD2 have certain associations with those type III bursts in higher frequency bands originating close to the Sun.

An overview of solar radio bursts in 06:00 to 09:30 UT on October 26 over the bands of 1 MHz–7.6 GHz is given in Figure 5. The radio emission started at about 06:13 UT with a group of fast type III bursts which extended over all of the radio

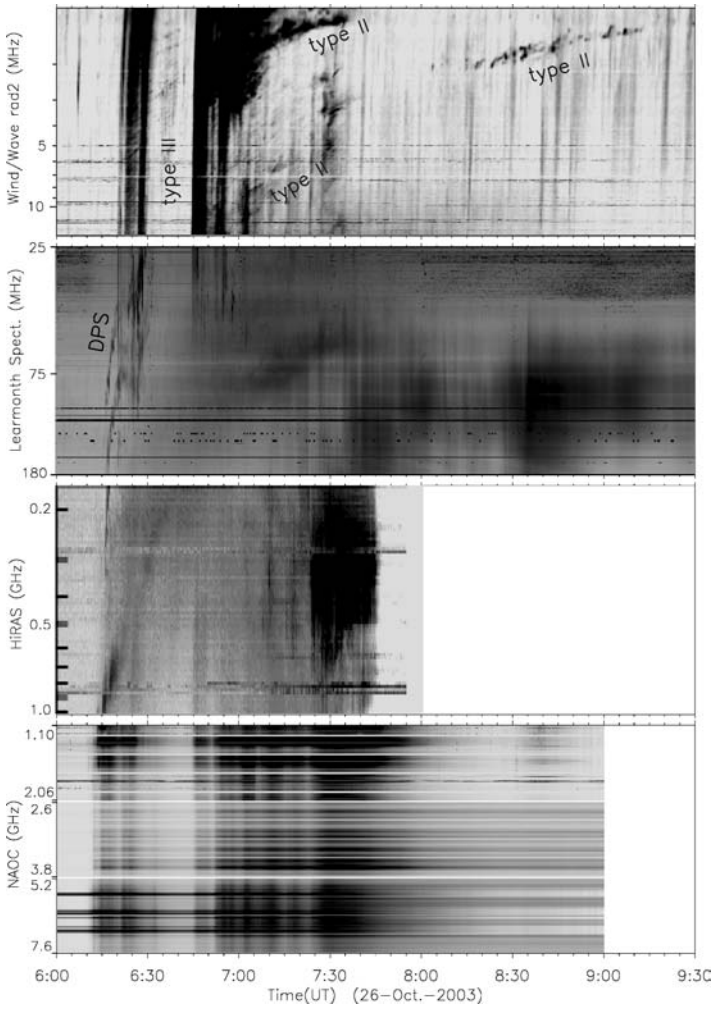

Figure 5. Dynamic spectrum of radio observations on October 26, 2003.

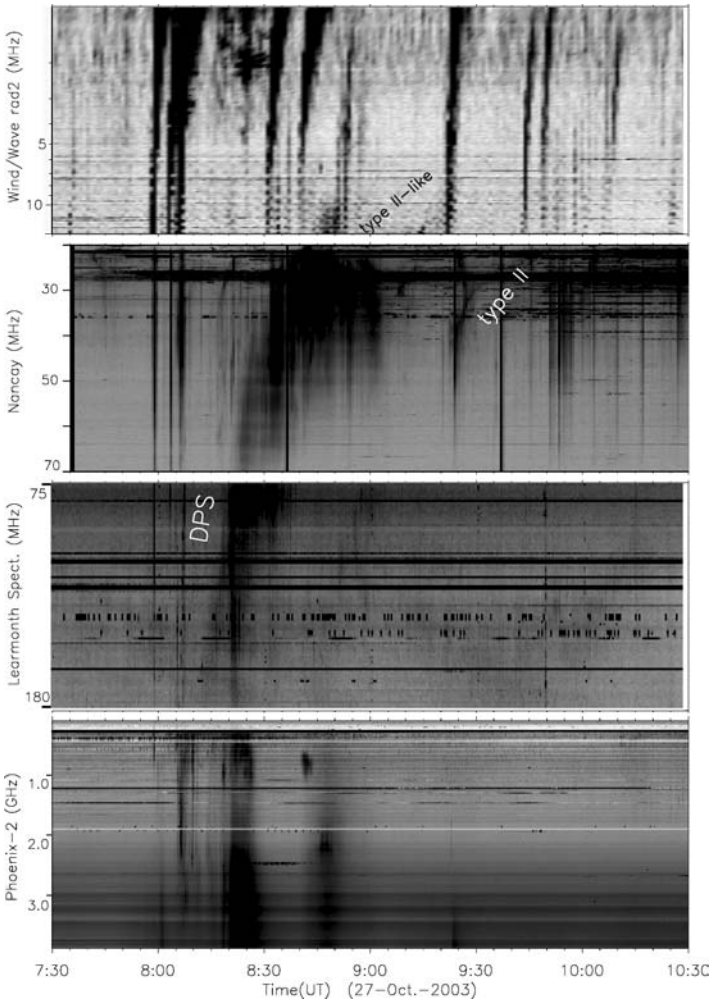

Figure 6. Dynamic spectrum of radio observations on October 27, 2003.

wavelength range at 16:15 UT. Meanwhile some DPSs were found in the range of 25 MHz–1.5 GHz. After 06:49 UT several interplanetary type II bursts were found which continued to about 09:12 UT. There were type IV bursts abroad in the range of microwave, the decimetric wavelength, the metric wavelength lasting more than 2.5 h. In short, this radio event included many complicated structures such as types IV, III, II bursts and DPSs. For the event in 17:00 to 21:30 UT on the same day, we have only the dynamic spectrum of Wind/Waves, which showed many clear fast type III bursts after about 17:30 UT and several distinguishable interplanetary type II bursts afterwards. However there were no higher frequency data for the event in the afternoon.

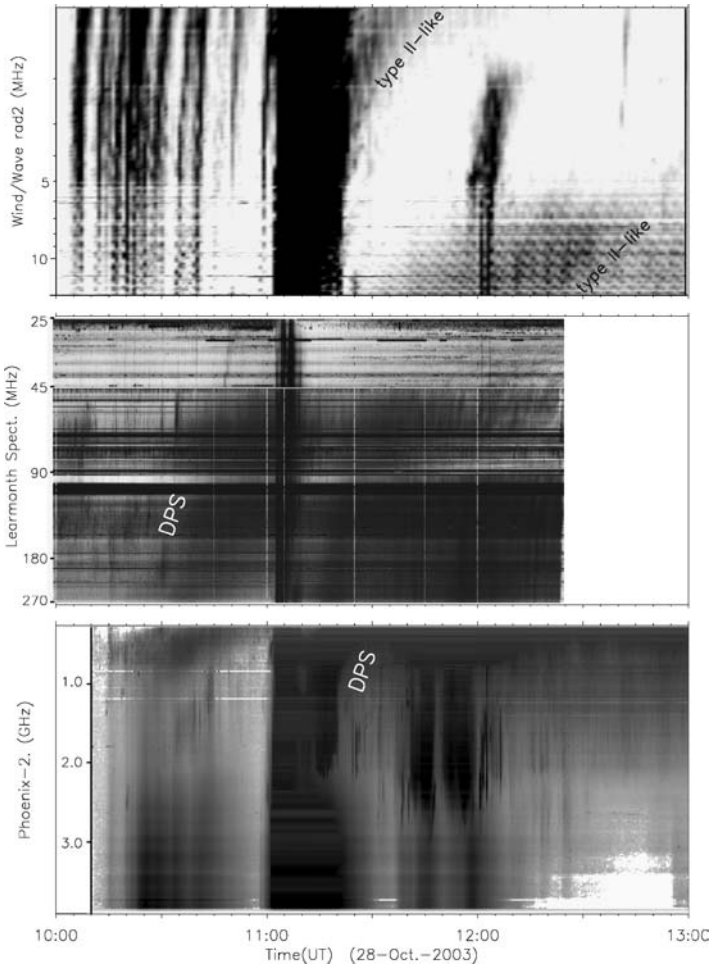

Figure 7. Dynamic spectrum of radio observations on October 28, 2003.

Figure 6 is for the sixth event on 27 October. A group of fast type III bursts was found after 07:58 UT over almost the whole radio range. At 08:07 UT first on the high-frequency part (nearly 1.0 GHz) DPS appeared, then the DPS drifted to the low-frequency part at nearly 20 MHz until 09:03 UT. Afterwards a type II burst was recorded by DAM/Nancay after 09:20 UT. Also in the range of 10–14 MHz, there seemed to be two slower drifting structures at about 08:45 and 09:15 UT. We called them type II-like bursts.

On 28 October there were many type III bursts and type IV emission appeared early at 10:00 UT (as seen in Figure 7). The broadband continuum emissions spread over the microwave, the decimetric wavelength, the metric wavelength lasting to about 12:30 UT. After 10:30 UT, a series of DPSs were found superposed on the background type IV bursts first at 1–2 GHz, and then drifting to metric wavelength.

Nearly at 11:00 UT a group of strong type III bursts spread from the low coronal region (high-frequency part) to interplanetary space. Afterwards at about 11:15 UT another group of DPSs began in 1–2 GHz, and then drifted to metric wavelength (nearly 45 MHz). In the range RAD2 of *Wind/Waves* there were some slower drifting structures at about 11:30 and 12:00 UT—type II-like bursts. This radio event was very complicated including types IV, III, II-like bursts and DPSs.

Finally, in the morning from 04:00 to 11:00 UT on October 29, there were no radio characteristics associated with a CME. In the afternoon 20:00 to 23:00 UT, we have only the dynamic spectrum of *Wind/Waves* which showed a group of strong fast type III bursts after about 20:38 UT and several distinguished type II bursts after 21:00 UT.

3.2. Solar energetic particle events

Not as complicated as the radio bursts, there were only three SEP events occurring at about 18:00 UT on 26, 12:00 UT on 28, and 21:00 on 29 October, respectively (as seen in the top panel of Figure 4). The peak intensities (I_p) of proton flux with energy >10 MeV were 380, 4590 and 2538 particles $cm^2\,s^{-1}\,ster^{-1}\,MeV^{-1}$, respectively, based on observations from the ACE spacecraft. Notably, the last two events were larger than the 'Bastille' event.

Obviously, the 3rd, 11th and 15th events listed in Table I should be responsible for these three SEP events. Each of these three events included a X-class flare and a fast frontside halo CME associated with a of filament eruption. Especially, in the last two events, the flares were extremely violent (X17.2 and X10.0), and the CMEs were extraordinary fast (2459 and 2029 $km\,s^{-1}$ approximately). These SEP events all lasted for durations more than one day, which indicate the presence of CME-driven shocks and that the shock acceleration is the main formation mechanism of energetic particles in the interplanetary medium (Reames, 1999).

Although the flare at 06:54 UT on October 26 was as intense as the flare at 17:54 UT, it did not produce a SEP event. This is because its location was S15E44 where the energetic particles cannot impact the Earth under the effect of the spiral interplanetary magnetic field (Cane, Reames, and von Rosenvinge, 1988; Reames, 1999).

3.3. Ejecta in the interplanetary medium

Figure 4 presents three relatively isolated ejecta (thereafter referred as Ejecta-I/II/III) arriving at 1 AU on 28, 29 and 30 October, respectively. The first ejecta (Ejecta-I) was the smallest among them (Figure 8). The driven shock arrived at 01:30 UT on October 28. After the shock the ratio of H_e^{++} to proton was high which indicates the corona ejecta (Hirshberg, Bame, and Robbins, 1972; Ogilvie and Hirshberg, 1974; Neugebauer, 1981; Neugebauer and Goldstein, 1997; Skoug

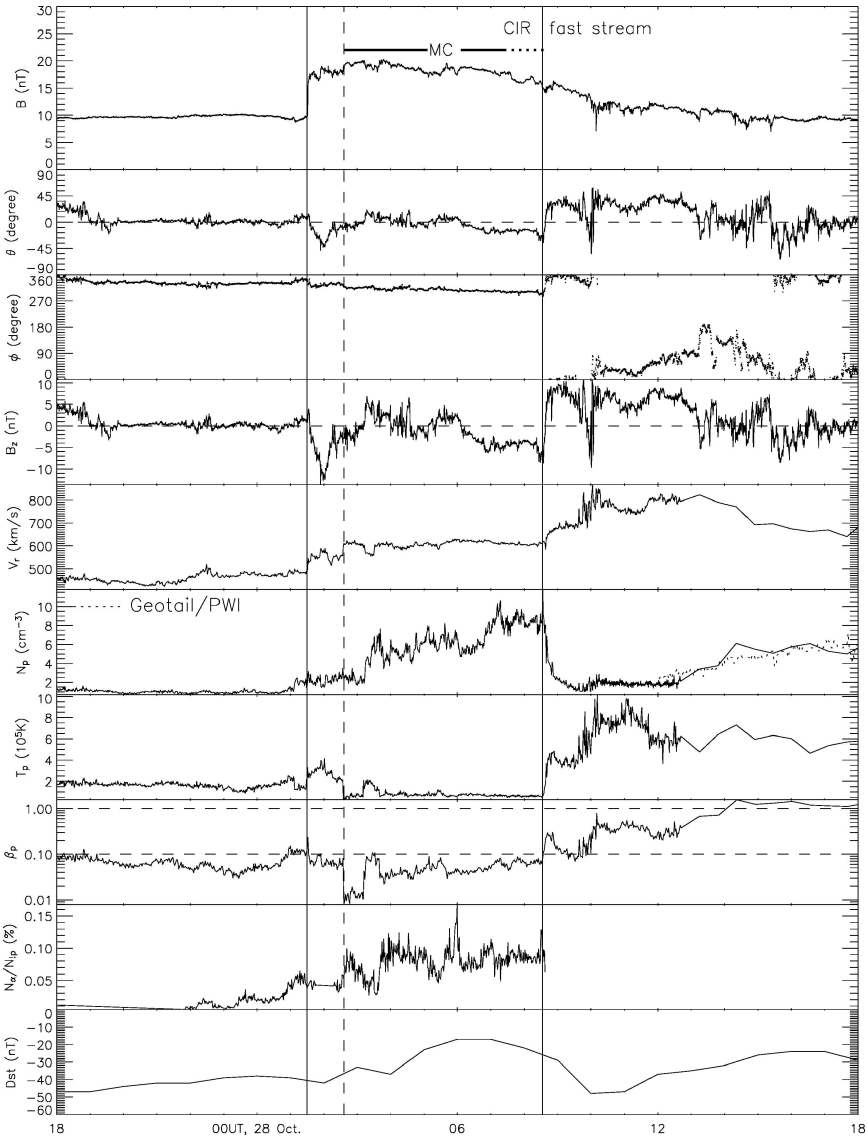

Figure 8. The interplanetary observations of magnetic field strength (B), the elevation (θ) and azimuth (ϕ) of field direction, the southward component (B_z) of magnetic field, solar wind speed (V_r), proton density (N_p), proton temperature (T_p), the ratio of proton thermal pressure to magnetic pressure (β_p) and the density ratio of H_e^{++} to proton (N_α/N_p) from the ACE spacecraft. The last panel shows the geomagnetic index (Dst).

et al., 1999). The ejecta was a magnetic cloud with a possible front boundary at 02:36 UT (as denoted by dashed line in Figure 8) where the proton temperature and β both decreased sharply and the rear boundary at 08:33 UT (as marked by the second solid line). Between the two boundaries, the magnitude of the field increased

and the field vector rotated smoothly from $\sim 10^\circ$ to $\sim -20^\circ$ in latitude. These are all the characteristics of a magnetic cloud (Burlaga *et al.*, 1981). Generally, a magnetic cloud can be locally modeled by a flux rope. In this model, if a spacecraft passes through the center of the magnetic cloud, the observed rotation of field vector will be close to 180°. However, the rotation inside Ejecta-I was small. This implies that only the flank or even the edge of it encountered the Earth. Moreover, the passage time of this cloud was much shorter than that of typical cloud ($\sim$1 day). It also implies that the observational spacecraft was far away from the axis of this magnetic cloud. We note the changes of parameters behind the cloud. The magnetic field orientation changed rapidly, the solar wind speed increased, the proton density decreased suddenly, and the temperature enhanced simultaneously. Roughly beginning from 27 October, the solar wind was always faster than 450 km s^{-1}. All of these signatures suggest that there was a fast stream following the magnetic cloud, and the cloud was pushed into a co-rotating interaction region (CIR) (Hundhausen, 1972; Smith and Wolf, 1976) ahead of this fast stream. The second solid line also denotes the interface between the slow solar wind and the following fast stream. Based on the above analysis, the solar source region of this cloud must be close to a large coronal hole from the west in terms of the Sun's rotation. As seen in the EIT 284 Å image (Figure 9), there was a large coronal hole to the east of AR10484 at that time. According to Table I, two halo CMEs (third and sixth events) to the west of the coronal hole were potentially corresponding to the cloud. However, there was too short a time for the sixth event to arrive at 1 AU. If the cloud was the counterpart of the sixth event, the average transit speed from the Sun to the Earth should be 2300 km s^{-1} larger than that of Ejecta-II whose transit speed was about

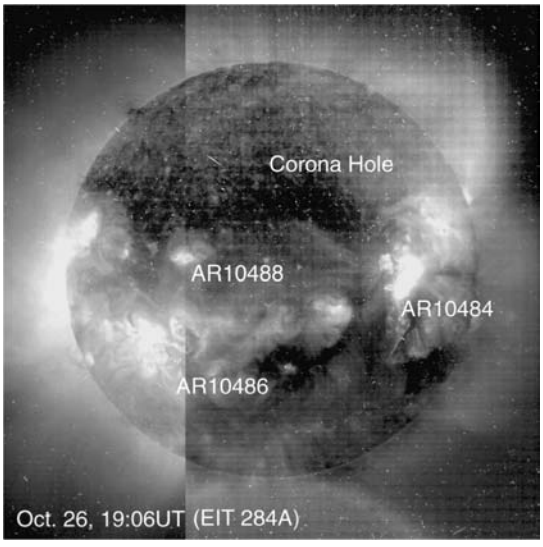

Figure 9. EIT 284Å image on October 26 shows the large corona hole.

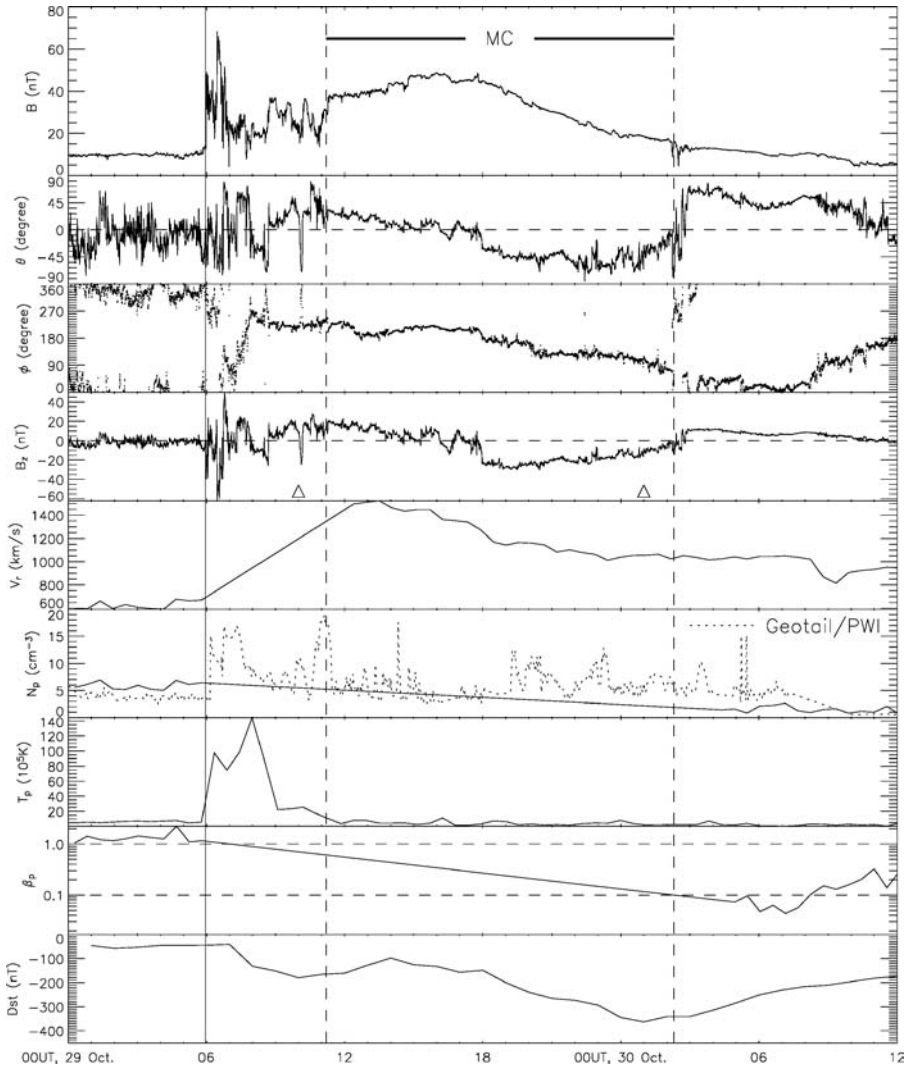

Figure 10. The interplanetary observations from the ACE spacecraft.

1770 km s^{-1} (as addressed in the next paragraph). This is impossible because such a large speed did not produce an even stronger shock. Thus, the third event, i.e. the CME that occurred at 17:54 UT on October 26, should be responsible for Ejecta-I, and the transit speed is estimated as $\sim$1270 km s^{-1}.

The reliability and resolution of solar wind plasma data was not good during the second ejecta (Ejecta-II, Figure 10). Although nothing could be concluded from the plasma data, we still believe that Ejecta-II was a typical magnetic cloud because the magnetic field perfectly satisfied the criteria of magnetic cloud: enhanced magnetic field strength and the large and smooth rotation of magnetic field vector (Burlaga

et al., 1981). The boundaries were at 11:00 UT on October 29 and 02:30 UT on October 30, between which the obvious field fluctuation vanished and the magnetic field rotated from north to south, from west to east. Ahead of the cloud, a strong driven shock appeared at 06:00 UT. It was the most intense forward shock during late October. According to Table I, the 11th event associated with a halo CME, which has an extremely fast speed, should be responsible for the magnetic cloud. It occurred at S16E08 approaching the meridian on October 28. If the correspondence is correct, the average transit speed of this ejecta was $\sim$1770 km s^{-1}. This is consistent with the CME's initial speed of 2459 km s^{-1}, which will decrease in the interplanetary medium. The 10th event is not likely to be the source of the cloud, because its initial speed ($\sim$1054 km s^{-1}) is too slow to arrive at 1 AU within so short an interval. However, since it preceded the next halo CME with only half an hour, we consider that there were two fates for it. One is that it had been consumed by the following fast large CME and therefore can not be distinguished at 1 AU; another is that it had been pushed to a side and even did not pass near the Earth. The sixth event was also not likely associated with the cloud, because it is not reasonable that the 6th event but not the 11th event produced the strongest shock at 1 AU.

The last ejecta (Ejecta-III) was also a large ejecta associated with a preceding strong shock at 16:30 UT on October 30 (Figure 11). The driven shock was weaker than the second one but stronger than the first one according to the sudden enhancement of magnetic field magnitude. This ejecta lasted from 02:00 UT on October 31 to 24:00 UT on November 1, where N_α/N_p was high and proton β was smaller than 0.1 approximately. The speed profile shows a single-transient, expanding fast flow. Nevertheless, the magnetic field within the ejecta was not as typical as that within magnetic cloud. Therefore, Ejecta-III was a magnetic cloud-like structure. Since Ejecta-II was associated with the violent CME on October 28 and there was only one frontside halo CME after it, obviously, the solar source of Ejecta-III was the violent CME on October 29. Its average transit speed from the Sun to 1 AU was $\sim$1440 km s^{-1} in the range of the transit speeds of Ejecta-I and Ejecta-II. This result is very consistent with the fact that, compared to the other two ejecta, Ejecta-III drove a moderate shock in the interplanetary medium.

3.4. GEOMAGNETIC STORMS

The geomagnetic index (*Dst*) shows that there were two major geomagnetic storms with *Dst* peak values less than -300 nT in late October. The first geomagnetic storm began the morning of October 29 and lasted until October 30. The bottom panel of Figure 10 shows the *Dst* index of this storm. Obviously, it was produced by Ejecta-II. The storm contained a double-peak structure, which has been studied in previous work (Kamide *et al.*, 1998; Jordanova *et al.*, 2003). One appeared at 10:00 UT on the 29th with a *Dst* peak value of -180 nT, which was caused by the shock sheath ahead of Ejecta-II. The southward component, B_s, of the magnetic

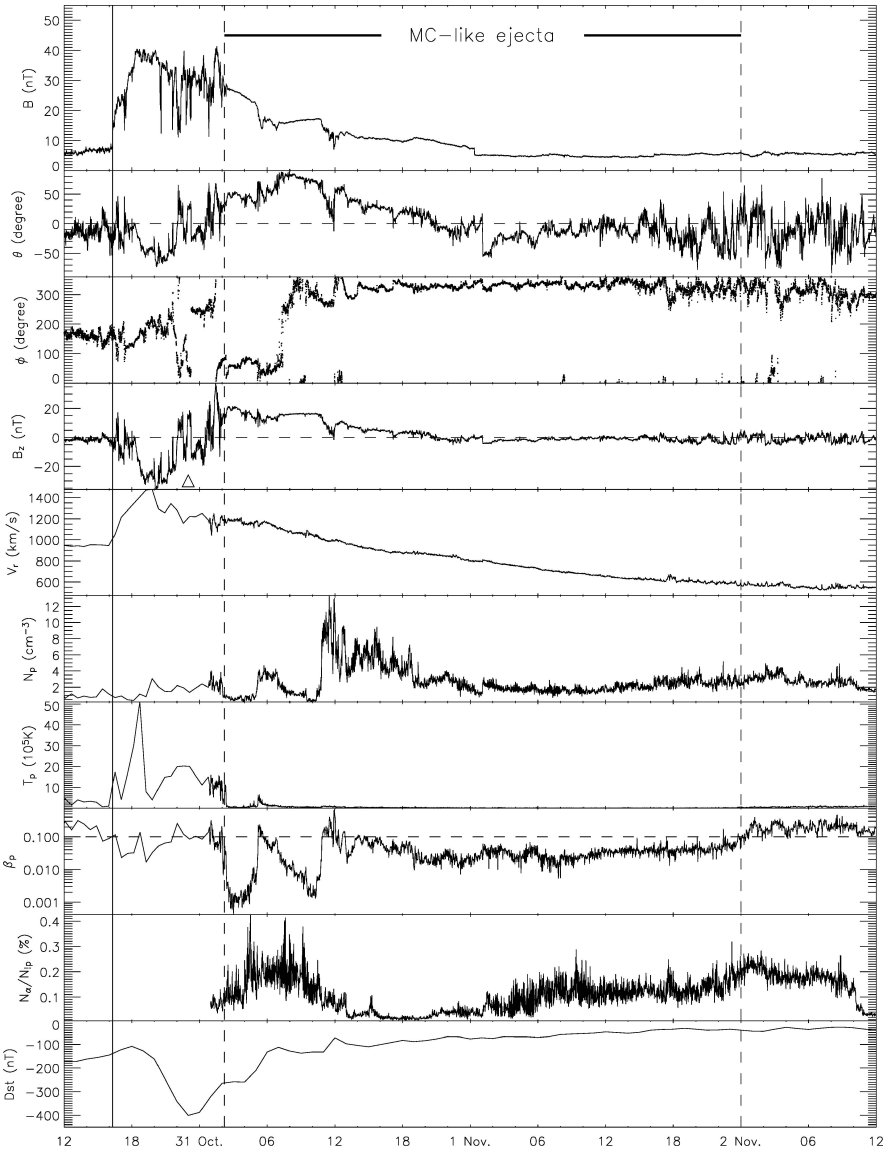

Figure 11. The interplanetary observations from the ACE spacecraft.

field inside the sheath even reached ∼60 nT. Although the duration of B_s was short, the extremely large value of B_s played a more important role in producing this *Dst* peak (Wang *et al.*, 2003). Another *Dst* peak appeared at 01:00 UT on the 30th with peak value of −363 nT, which was produced by the long B_s intrinsic to Ejecta-II. Compared to the B_s inside the shock sheath, the magnitude was less (nearly 30 nT), but the duration was much longer (more than 7 h). Very long B_s durations may also produce very large geomagnetic storms.

The second geomagnetic storm just followed the first one that did not yet recover to quiet phase completely. It began at about 18:00 UT on October 30 (Figure 11). Basing on the earlier storm, the *Dst* value reached −401 nT during this storm. It was caused by the B_s inside the shock sheath preceding Ejecta-III. The maximum value of B_s was about 32 nT and lasted about 4 h. In addition, Figure 8 shows that Ejecta-I only caused a small geomagnetic disturbance. Since B_s inside Ejecta-I was very small (<10 nT), the *Dst* peak value was only −48 nT.

4. Summary and Discussion

In summary, a total of nine M-class, four X-class X-ray flares and six frontside halo CMEs, among which three were associated with obvious filament eruptions, occurred during October 26–29. They caused many type II, III, IV radio bursts and DPSs, three large SEP events, three ejecta with shocks preceding, and two great geomagnetic storms. Table II clearly gives the relations between the major solar events and the interplanetary responses.

All of the flares were associated with type III radio bursts, all of the frontside halo CMEs were accompanied by type II or type II-like radio bursts, and in some events, DPS and type IV radio bursts can be observed. Except for the first X-class flare, all of the X-class flares combined with fast frontside halo CMEs caused extraordinary enhancements of solar energetic particle flux near the Earth. These fast CMEs were all associated with filament eruptions. In addition to the SEPs, the three filament-associated CMEs produced the only three ejecta including at least two magnetic clouds in the interplanetary medium. The last two ejecta, which were

TABLE II

The major solar activities and their interplanetary responses in late October 2003.

No.	Major solar activities	Interplanetary responses
1	X1.2 flare; CME ($V_i \approx 1370$ km s^{-1}[a]); no FE[b]	DPS[c], types II, III, IV
3	X1.2 flare; CME ($V_i \approx 1537$ km s^{-1}); FE	types II, III; SEP[d]; MC[e]
6	M2.7 flare; CME ($V_i \approx 1322$ km s^{-1}); no FE	DPS, types II, III
11	X17.2 flare; full halo CME ($V_i \approx 2459$ km s^{-1}); FE	DPS, type II-like, III, IV; SEP ($I_p > 1000$); MC; $Dst = -363$ nT
15	X10.0 flare; full halo CME ($V_i \approx 2029$ km s^{-1}); FE	types II, III; SEP ($I_p > 1000$); MC-like ejecta; $Dst = -401$ nT

[a]Initial projected speed of CME.
[b]Filament eruption.
[c]Drifting pulsation structure.
[d]Solar energetic particle event.
[e]Magnetic cloud.

related to the two super X-ray flares, two extremely fast halo CMEs and two large SEP events, created the two great geomagnetic storms with *Dst* values of −363 and −401 nT, respectively. Evidently, although there were many solar activities in late October 2003, only several notable events should be responsible for the great disturbances near the Earth.

Multiple-magnetic-cloud (Multi-MC) structures are formed likely due to the overtaking of successive CMEs in the interplanetary medium (Wang, Wang, and Ye, 2002; Wang, Ye, and Wang, 2003; Hu *et al.*, 2004). For example, the March 31 event and April 11–14, 2001 event were both cases of Multi-MC. In those events, the Multi-MC-associated CMEs originated from almost the same solar region, and were initially separated from each other by approximately half a day. However, in the late October events, no Multi-MC was formed though there were many CMEs. The two large interplanetary ejecta corresponding to the October 28 and 29 violent halo CMEs were still relatively isolated even at 1 AU. According to the observations and the simulation by Wang *et al.* (2004b), to get a Multi-MC requires at least two conditions: (1) the latter CME should be faster than the former, and (2) they should be separated by a moderate interval at the beginning. Obviously, neither is satisfied for the two violent CMEs. They were separated for too long (∼33 h at the beginning) and the second CME was slower than the first one.

SEP events and geomagnetic storms are the two most important aspects affecting the space weather near the Earth. Generally, shock wave acceleration is considered a main mechanism of the formation of solar energetic particles (Reames, 1999). In the late October events, the peak intensity of these three SEP events increased with the increase of the associated shock strength at 1 AU. The second SEP event was the largest, and the associated CME was the fastest with average transit speed of ∼1770 km s^{-1} from the Sun to 1 AU. The first SEP event was the smallest, and the transit speed of the associated CME was ∼1270 km s^{-1}. The third SEP event was associated with a ∼1440 km s^{-1} CME. Particularly, in comparison of the second and third SEP events, the difference between the influences of the two CME's location is small because these two SEP-associated CMEs (the 11th and 15th events) both originated from AR10486 with solar surface location of E08 and W02, respectively.

However, an interplanetary shock is very complicated and to obtain its real shock speed is difficult, so that no pure association between CME-driven shock speeds and peak SEP intensities is established (Reames, 2000; Kahler and Reames, 2003; Kahler, 2004). Moreover, the existence of enough energetic seed particles is necessary for the shock acceleration process (Kahler, 2001). Hence, the background solar wind from different solar regions may influence the formation of SEPs. In addition, the situations between perpendicular and parallel shock are different. So the longitude of CMEs is also an important factor for the SEP intensity (Cane, Reames, and von Rosenvinge, 1988; Reames, 1997).

As a main creator of geomagnetic storms, the interplanetary ejecta and their associated shocks observed during this period were all related to the filament-associated

CMEs according to Table II. Since a magnetic cloud is a consequence of a coronal mass ejection that contains a great amount of magnetic field from the corona, the magnetic helicity between the cloud and its solar source must have some relation.

Statistically, the dextral filaments are dominant in the northern solar hemisphere and the sinistral filaments are dominant in the southern hemisphere (Martin, Bilimoria, and Tracadas, 1994; Martin and McAllister, 1996). Similarly, there are two categories of coronal arcades overlying filaments and named them "left-skewed" and "right-skewed". The dextral filaments are associated with left-skewed arcades yielding left-hand (negative) helicity and the sinistral filaments are associated with right-skewed arcades yielding right-hand (positive) helicity (Martin and McAllister, 1997). Some models set up the relationship that the eruption of dextral filaments will result in negative-helical CMEs; eruption of sinistral filaments will result in positive-helical CMEs. Thus, negative- and positive-helical interplanetary magnetic clouds would be expected to come from northern and southern solar hemisphere (Martin and McAllister, 1996; Rust and Kumar, 1994). This conclusion is supported by many observations (Rust, 1994; Bothmer and Schwenn, 1994; Pevtsov, Canfield, and Metcalf, 1995; Ruzmaikin, Martin, and Hu, 2003).

However, the largest magnetic cloud (Ejecta-II) on October 29, which came from the southern hemisphere, does not obey the statistical rule. We use two methods to examine the sign of helicity of the magnetic cloud. The first approach is as the description in the Ruzmaikin, Martin, and Hu (2003), and Matthaeus and Goldstein (1982) works. The information about the magnetic helicity is stored in the cross-correlation of different components of the magnetic field, $C(\delta t) = \langle B_z(t) B_y(t+\delta t) \rangle$, and the sign of helicity is as the same as the slope of the $C(\delta t)$ at $\delta t = 0$. Figure 12 shows the profile of C that suggests that the helicity of the cloud is negative, contrary to the regular pattern. Another method is to fit the observed data to a force-free cylindrical flux rope described by the Lundquist solution (Lundquist, 1950). Seven parameters include the sign of magnetic helicity are fitted (Lepping, Jones, and Burlaga, 1990). The result is presented in Figure 13. Consistent with the first method, the estimated helicity of the cloud is also negative. Moreover, the

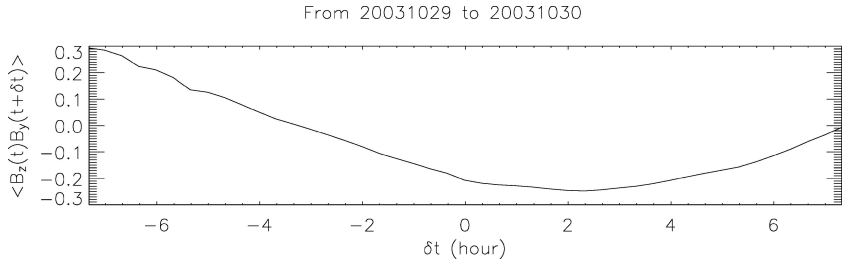

Figure 12. Cross-correlation as a function of δt for Ejecta-II. The sign of helicity is the same as the slope of the curve at $\delta t = 0$.

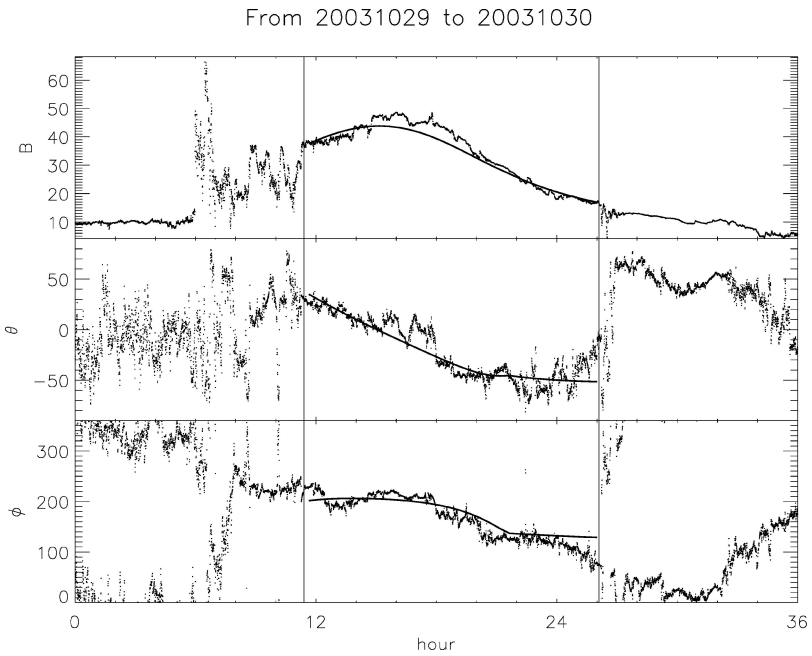

Figure 13. The fitting results of Ejecta-II by using a force-free cylindrical flux rope model. The estimated helicity is left-handed, and the orientation of the cloud is at 246° longitude and −12° latitude approximately in GSE coordinates.

orientation, i.e., the direction of the axial magnetic field, of the cloud is estimated as approximately 246° longitude and −12° latitude.

For the effect of the magnetic cloud on the geomagnetic disturbance, its orientation is important (Zhao, 2002; Zhao and Webb, 2003). Although there is an association of the sign of helicity between interplanetary magnetic clouds and their solar sources—CMEs and filaments, whether one can estimate the orientation of a magnetic cloud by regarding the associated filament is not known. For Ejecta-II, the axis of the cloud seems to be along the direction of the associated erupted filament which was from northeast to southwest. However, the orientations of magnetic clouds are not always consistent with the directions of associated filaments. Occasionally, deviation between them is significant, e.g., the November 20, 2003 event analyzed by Wang *et al.* (2004a). The angle between the orientations of the magnetic cloud and its associated filament was ∼51° in that event. Thus, it is necessary to further understand the relationship between magnetic clouds and their associated filaments.

Acknowledgements

We acknowledge the use of the data from SOHO, ACE and *Wind* spacecraft, the H_α data from the YNAO, the radio dynamic spectrum from Huairou/China,

Nancay/France, Learmonth Spectrograph/Australia, Hiraiso/Japan and Phoenix-2/Switzerland, and the *Dst* index from World Data Center. We thank Dr. R. Skoug, Dr. T. Terasawa, Dr. T. Zurbuchen, and Dr. J. Raines for providing the best available solar wind plasma data during October 28–30. We also thank the referee for constructive comments. This work is supported by the Chinese Academy of Sciences (KZCX2-SW-136), the National Natural Science Foundation of China (40404014, 40336052, 40336053), and the State Ministry of Science and Technology of China (G2000078405).

References

Bothmer, V. and Schwenn, R.: 1994, *Space Sci. Rev.* **70**, 215.

Burlaga, L. F., Plunkett, S. P., and St. Cyr, O. C.: 2002, *J. Geophys. Res.* **107**, 1266 doi:10.1029/2001JA000255.

Burlaga, L., Sittler, E., Mariani, F., and Schwenn, R.: 1981, *J. Geophys. Res.* **86(A8)**, 6673.

Burlaga, L. F., Skoug, R. M., Smith, C. W., Webb, D. F., Zurbuchen, T. H., and Reinard, A.: 2001, *J. Geophys. Res.* **106**, 20957.

Cane, H. V., Reames, D. V., and von Rosenvinge, T. T.: 1988, *J. Geophys. Res.* **93**, 9555.

Gonzalez, W. D., and Tsurutani, B. T.: 1987, *Planet. Space Sci.* **35**, 1101.

Hirshberg, J., Bame, S. J., and Robbins, E. E.: 1972, *Solar Phys.* **23**, 467.

Hu, Q., Smith, C. W., Ness, N. F., and Skoug, R. M.: 2004, *J. Geophys. Res.* **109**(A3), A03102.

Hundhausen, A. J.: 1972, *Coronal Expansion and Solar Wind*, Vol. 238, Springer-Verlag, New York.

Jordanova, V. K., Kistler, L. M., Thomsen, M. F., and Mouikis, C. G.: 2003, *Geophys. Res. Lett.* **30**(6), 1311 doi:10.1029/2002GL016576.

Kahler, S. W.: 2001, *J. Geophys. Res.* **106**(A10), 20947.

Kahler, S. W.: 2004, *Astrophys. J.* **603**, 330.

Kahler, S. W. and Reames, D. V.: 2003, *Astrophys. J.* **584**, 1063.

Kamide, Y., Yokoyama, N., Gonzalez, W. D., Tsurutani, B. T., Brekke, A., and Masuda, S.: 1998, *J. Geophys. Res.* **103**, 6917.

Lepping, R. P., Berdichevsky, D. B., Burlaga, L. F., Lazarus, A. J., Kasper, J., Desch, M. D., Wu, C.-C., Reames, D. V., Singer, H. J., Smith, C. W., and Ackerson, K. L.: 2001, *Solar Phys.* **204**, 285.

Lepping, R. P., Jones, J. A., and Burlaga, L. F.: 1990, *J. Geophys. Res.* **95**, 11957.

Lundquist, S.: 1950, *Ark. Fys.* **2**, 361.

Martin, S. F., Bilimoria, R., and Tracadas, P. W.: 1994, in R. Rutten and C. J. Schrijver (eds.), *Solar Surface Magnetism*, Kluwer Academic Publishers, Dordrecht, p. 303.

Martin, S. F. and McAllister, A. H.: 1996, in Y. Uchida, H. S. Hudson, and T. Kosugi (eds.), *Magnetohydrodynamic Phenomena in the Solar Atmosphere, Prototypes of Stellar Magnetic Activity*, Kluwer Academic Publishers, Dordrecht, p. 497.

Martin, S. F. and McAllister, A. H.: 1997, in N. Crooker, J. Joselyn, and J. Feynman (eds.), *Coronal Mass Ejections*, Dordrecht, p. 127.

Matthaeus, W. H. and Goldstein, M. L.: 1982, *J. Geophys. Res.* **87**, 6011.

Neugebauer, M.: 1981, *Fundam. Cosmic Phys.* **7**, 131.

Neugebauer, M. and Goldstein, R.: 1997, in N. Crooker, J. A. Joselyn, and J. Feynman (eds.), *Coronal Mass Ejections*, Washington, DC, p. 245.

Nitta, N. V. and Hudson, H. S.: 2001, *Geophys. Res. Lett.* **28**, 3801.

Ogilvie, K. W. and Hirshberg, J.: 1974, *J. Geophys. Res.* **79**, 4595.

Pevtsov, A. A., Canfield, R. C., and Metcalf, T. R.: 1995, *Astrophys. J.* **440**, L109.
Reames, D. V.: 1997, in N. Crooker, J. A. Joselyn, and J. Feynman (eds.), *Coronal Mass Ejections*, p. 217.
Reames, D. V.: 1999, *Space Sci. Rev.* **90**, 413.
Reames, D. V.: 2000, in B. L. Dingus, D. B. Kieda, and M. H. Salamon (eds.), *Invited, Rapporteur, and Highlight Papers*, *AIP Conf. Proc.* **516** 289.
Rust, D. M.: 1994, *Geophys. Res. Lett.* **21**, 241.
Rust, K. and Kumar, A.: 1994, *Solar Phys.* **155**, 69.
Ruzmaikin, A., Martin, S., and Hu, Q.: 2003, *J. Geophys. Res.* **108**(A2), 1096.
Skoug, R. M., Bame, S. J., Feldman, W. C., Gosling, J. T., McComas, D. J., Steinberg, J. T., Tokar, R. L., Riley, P., Burlaga, L. F., Ness, N. F., and Smith, C. W.: 1999, *Geophys. Res. Lett.* **26**, 161.
Smith, C. W., Ness, N. F., Burlaga, L. F., Skoug, R. M., McComas, D. J., Zurbuchen, T. H., Gloeckler, G., Haggerty, D. K., Gold, R. E., Desai, M. I., Mason, G. M., Mazur, J. E., Dwyer, J. R., Popecki, M. A., Mobius, E., Cohen, C. M. S., and Leske, R. A.: 2001, *Solar Phys.* **204**, 227.
Smith, E. J. and Wolf, J. W.: 1976, *Geophys. Res. Lett.* **3**, 137.
Tsurutani, B. T., Gonzalez, W. D., Tang, F., Akasofu, S. I., and Smith, E. J.: 1988, *J. Geophys. Res.* **93**, 8519.
Wang, Y., Shen, C. L., Wang, S., and Ye, P. Z.: 2003, *Geophys. Res. Lett.* **30**(20), 2039.
Wang, Y., Zheng, H., Wang, S., and Ye, P.: 2004b, *Astron. Astrophys.*, in press.
Wang, Y., Zhou, G., Ye, P., Wang, S., and Wang, J.: 2004a, in *Coronal and Stellar Mass Ejections, IAU Symposium No. 226*, Beijing, China.
Wang, Y. M., Wang, S., and Ye, P. Z.: 2002, *Solar Phys.* **211**, 333.
Wang, Y. M., Ye, P. Z., and Wang, S.: 2003, *J. Geophys. Res.* **108**(A10), 1370.
Wang, Y. M., Ye, P. Z., Wang, S., Zhou, G. P., and Wang, J. X.: 2002b, *J. Geophys. Res.* **107**(A11), 1340.
Webb, D. F., Cliver, E. W., Crooker, N. U., St. Cyr, O. C., and Thompson, B. J.: 2000, *J. Geophys. Res.* **105**(A4), 7491.
Zhao, X. P.: 2002, in H. Wang and R. Xu (eds.), *Proceedings of the COSPAR Colloquium Held in the NAOC in Beijing, China*, p. 209.
Zhao, X. P. and Webb, D. F.: 2003, *J. Geophys. Res.* **108**(A6), 1234.